RDA-TR-144200-002

SEPTEMBER 1988

ANNUAL TECHNICAL REPORT FOR CONTRACT F49620-87-C-0117

For Period 1 September 1987 to 31 August 1988

MPD ARCJET THRUST CHAMBER FLOW DYNAMICS

Prepared for:

DEPARTMENT OF THE AIR FORCE
AIR FORCE OFFICE OF SCIENTIFIC RESEARCH
BOLLING AFB, DC 20332-6448

Prepared by:

RDA/WRL Staff

RDA

R&D ASSOCIATES

301A SOUTH WEST STREET, ALEXANDRIA, VIRGINIA 22314 • (703) 684-0333

UNCLASSIFIED
SECURITY CLASSIFICATION OF THIS PAGE

REPORT DOCUMENTATION PAGE

Form Approved
OMB No. 0704-0188

1a. REPORT SECURITY CLASSIFICATION unclassified	1b RESTRICTIVE MARKINGS
2a. SECURITY CLASSIFICATION AUTHORITY	3. DISTRIBUTION/AVAILABILITY OF REPORT approved for public release, distribution is unlimited
2b. DECLASSIFICATION/DOWNGRADING SCHEDULE	
4. PERFORMING ORGANIZATION REPORT NUMBER(S)	5. MONITORING ORGANIZATION REPORT NUMBER(S) AFOSR-TR- 88-1183
6a. NAME OF PERFORMING ORGANIZATION R & D Associates, Inc.	6b. OFFICE SYMBOL (If applicable) RDA/WRL
7a. NAME OF MONITORING ORGANIZATION AFOSR/NA	
6c. ADDRESS (City, State, and ZIP Code) 301A S. West St. Alexandria, VA 22314	7b. ADDRESS (City, State, and ZIP Code) Building 410, Bolling AFB, DC 20332-6448
8a. NAME OF FUNDING/SPONSORING ORGANIZATION AFOSR/NA	8b. OFFICE SYMBOL (If applicable) NA
9. PROCUREMENT INSTRUMENT IDENTIFICATION NUMBER F49620-86-C-0117	
8c. ADDRESS (City, State, and ZIP Code) Building 410, Bolling AFB, DC 20332-6448	10. SOURCE OF FUNDING NUMBERS PROGRAM ELEMENT NO. 61102F; PROJECT NO. 2308; TASK NO. 001AB OPT. 1; WORK UNIT ACCESSION NO.

11. TITLE (Include Security Classification)
(U) MPD Thrust Chamber Flow Dynamics

12. PERSONAL AUTHOR(S)

13a. TYPE OF REPORT	13b. TIME COVERED	14. DATE OF REPORT (Year, Month, Day)	15. PAGE COUNT
~~Final~~	FROM 1 OCT87 TO 30SEPT88	88-09-29	29

16. SUPPLEMENTARY NOTATION

17. COSATI CODES			18. SUBJECT TERMS (Continue on reverse if necessary and identify by block number)
FIELD	GROUP	SUB-GROUP	Electric propulsion, magnetoplasmadynamic, arcjet ARC JET ENGINES, SPACE PROPULSION. (JES)

19. ABSTRACT (Continue on reverse if necessary and identify by block number)

Magnetoplasmadynamic (MPD) arcjet thrusters inherently involve close coupling of the electromagnetic discharge structure and the flow field in the thrust chamber. The discharge and internal flow field structures are not simply determined by the arcjet geometry, but depend on the values and partitioning of injected mass flow for each operating current condition. In order to understand the internal flow dynamics of an MPD arcjet, experiments are performed in which electromagnetic fields and flow properties are measured within the thrust chamber. Electric and magnetic field probes are used to obtain the electromagnetic structure, while spectroscopic techniques are used to estimate particle velocities and densities.

Results from the past year's effort include measurements of Doppler widths in argon and hydrogen as functions of position in the thruster for two arrangements of mass injection: 100% at backplate mid-radius and 50-50% at backplate mid-radius and cathode base. Reduced data suggest that a substantial radial component of flow exists in the

20. DISTRIBUTION/AVAILABILITY OF ABSTRACT ☒ UNCLASSIFIED/UNLIMITED ☒ SAME AS RPT. ☒ OTIC USERS	21. ABSTRACT SECURITY CLASSIFICATION Unclassified
22a. NAME OF RESPONSIBLE INDIVIDUAL Dr. Mitat Birkan	22b. TELEPHONE (Include Area Code) (202) 767-4938
	22c. OFFICE SYMBOL AFOSR/NA

DD Form 1473, JUN 86 — Previous editions are obsolete. — SECURITY CLASSIFICATION OF THIS PAGE
UNCLASSIFIED

RDA-TR-144200-002 SEPTEMBER 1988

ANNUAL TECHNICAL REPORT

For period 1 October 1987 to 30 September 1988

MPD THRUST CHAMBER FLOW DYNAMICS

Prepared for:

DEPARTMENT OF THE AIR FORCE
AIR FORCE OFFICE OF SCIENTIFIC RESEARCH
BOLLING AIR FORCE BASE, DC 20332-6448

Prepared by:

RDA/WRL Staff

TABLE OF CONTENTS

LIST OF ILLUSTRATIONS

I. SUMMARY

Magnetoplasmadynamic (MPD) arcjet thrusters inherently involve close coupling of the electromagnetic discharge structure and the flow field in the thrust chamber. The discharge and internal flow field structures are not simply determined by the arcjet geometry, but depend on the values and partitioning of injected mass flow for each operating current condition. In order to understand the internal flow dynamics of an MPD arcjet, experiments are performed in which electromagnetic fields and flow properties are measured within the thrust chamber. Electric and magnetic field probes are used to obtain the electromagnetic structure, while spectroscopic techniques are used to estimate particle velocities and densities.

Results from the past year's effort include measurements of Doppler widths in argon and hydrogen as functions of position in the thruster for two arrangements of mass injection: 100 % at backplate mid-radius and 50-50% at backplate mid-radius and cathode base. Reduced data suggest that a substantial radial component of flow exists in the former case, while little radial flow is indicated for the latter case. Radial flow could result in significantly inceasing shock and/or viscous losses near the cathode. Performance improvements in MPD arcjets would thus depend on properly matching the thrust chamber injector geometry to the flow field actually obtained with particular choices of total current and mass flow.

II. INTRODUCTION

The magnetoplasmadynamic (MPD) arcjet has attracted attention for many years because of its promise for providing a high thrust density, high specific impulse space propulsion technique. A particularly important characteristic of the MPD arcjet, (in contrast to electostatic thrusters), is the simplicity of the electrode/channel structure accelerating and guiding the thruster flow. While the solid structures of the MPD thruster can be quite simple (e.g., two coaxial electrodes), the internal flow of plasma in the thrust chamber may be very complex since the MPD flow inherently depends on close interaction of the electromagnetic discharge and flow structures. These flow structures are not simply determined by the thrust chamber geometry but can vary with changes in overall operating parameters such as current and rate of mass flow injection. In order to understand the performance characteristics of MPD arcjets, it is necessary to determine the electromagnetic discharge and flow structures within the thrust chamber. Such determination requires diagnosis of electromagnetic field distributions and measurement of the particle densities and velocities in the thrust chamber flow.

The present research program is directed toward diagnosing the MPD thrust chamber flow and comparing the measured electromagnetic and flow structures with theoretical predictions (e.g. MHD code results). The electromagnetic structure is obtained by internal electric and magnetic probe techniques. Non-intrusive optical techniques, particularly time-and spatially-resolved spectroscopy, provide measures of the particle velocities and chemical states. In addition to experimental measurements, a set of calculations using the MACH2 two-dimensional MHD code [1] has been started based on the actual arcjet geometry and operating parameters of the experiment.

III. PROGRESS

In the past year, a new MPD arcjet system was installed and tested. The device, shown in Figure 1, has a brass outer anode 8.41 cm ID and a copper-tungsten alloy cathode 3.81 cm OD. The channel length is 5 cm from the boron nitride insulator backplate to the exit plane. Argon or argon-hydrogen mixtures were delivered to the arcjet through 16 choked orifices in the boron nitride backplate at the mid-radius of the channel gap. Current is delivered to the arcjet from the PFN with a pulse width of 0.8 ms and peak currents of up to 45 kA.

A consistent set of operating conditions were used for magnetic probe and spectroscopic measurements. The PFN was charged to 8 kV and the gas flow rate was 6 g/s (argon with 1.5 percent added hydrogen). Figure 2 shows the current waveform for these conditions. The quasi-steady current is approximately 20 kA. The arcjet breech voltage, Figure 3, attains a quasi-equilibrium value of 50 V for approximately 400 μs about 200 μs after current initiation. Two magnetic field probes were used to map the enclosed current contours. Over 70 data shots, at two data points per shot, were taken to map 60 locations in the arcjet thrust chamber. Figure 4 shows the enclosed current contours in the arcjet operating at 20 kA and 6 g/s. Note that the current distribution is basically retained within the thrust chamber, with less than 5 percent of the total current beyond the exit plane. There are also indications that near the boron nitride backplate at the midchannel gas inlet ports the current distribution is perturbed, possibly in response to the entry of relatively high density, low speed flow into the thrust chamber. The $\bar{j} \times \bar{B}$ forces on the plasma have significant radial components near the anode and cathode suggesting radial velocity components and indicating possible increases in plasma density towards the conductor surfaces, particularly the cathode.

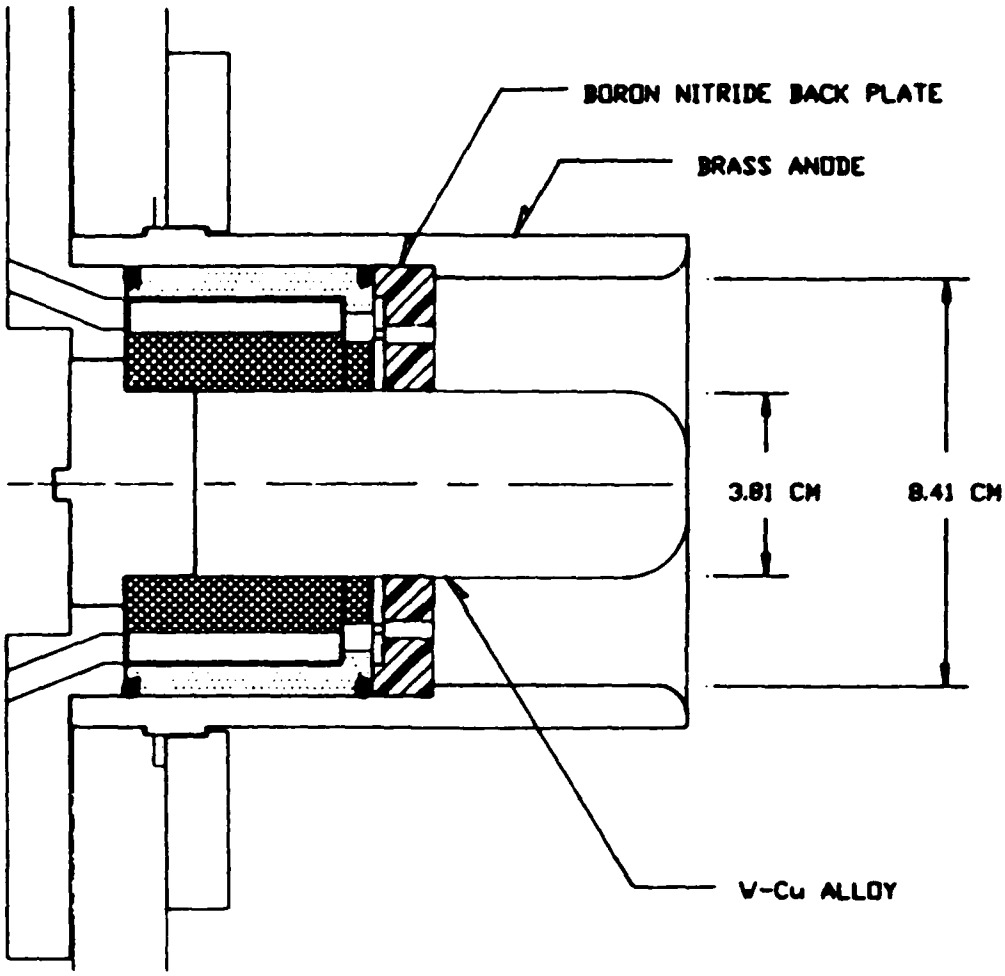

Figure 1. Schematic of new MPD arcjet for study of MPD thrust chamber flow dynamics. Gas injection is through 16 choked orifices at mid-radius in boron nitride backplate.

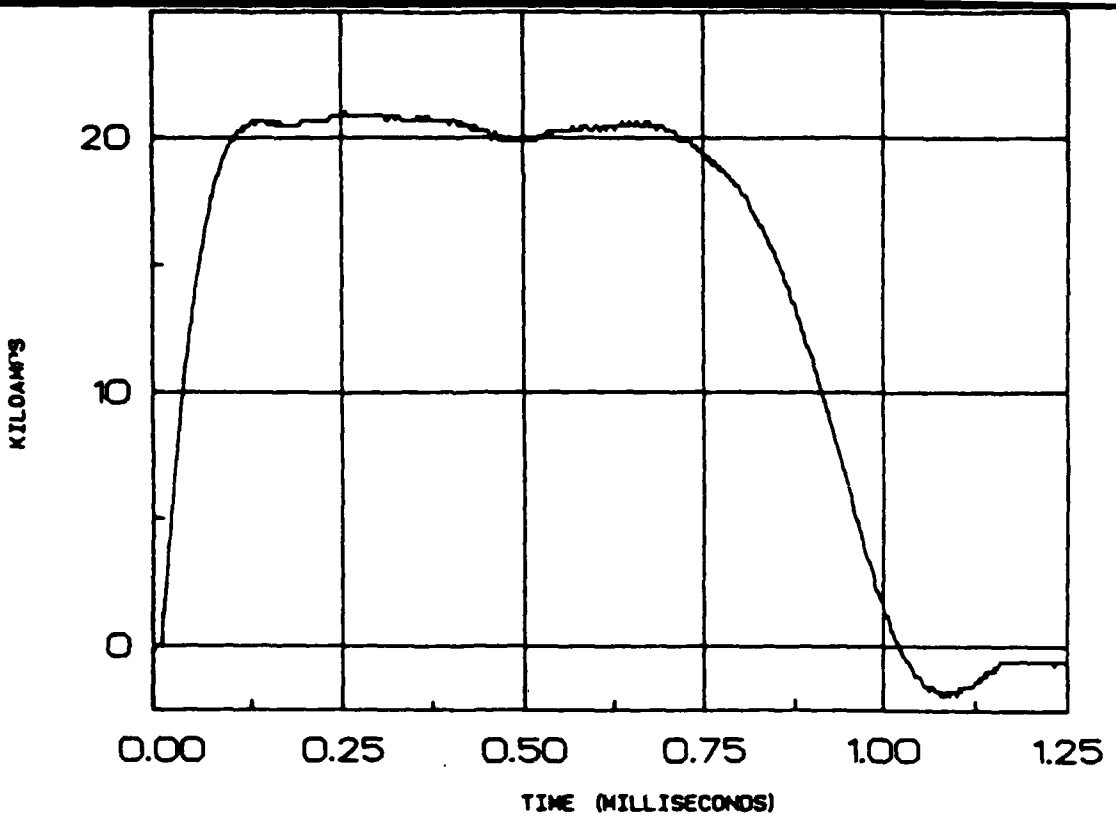

Figure 2. Current delivered to the MPD arcjet has a FWHM of 900 μs with a risetime of 100 μs. An initial voltage of 8 kV on the PFN gives a current of approximately 20 kA.

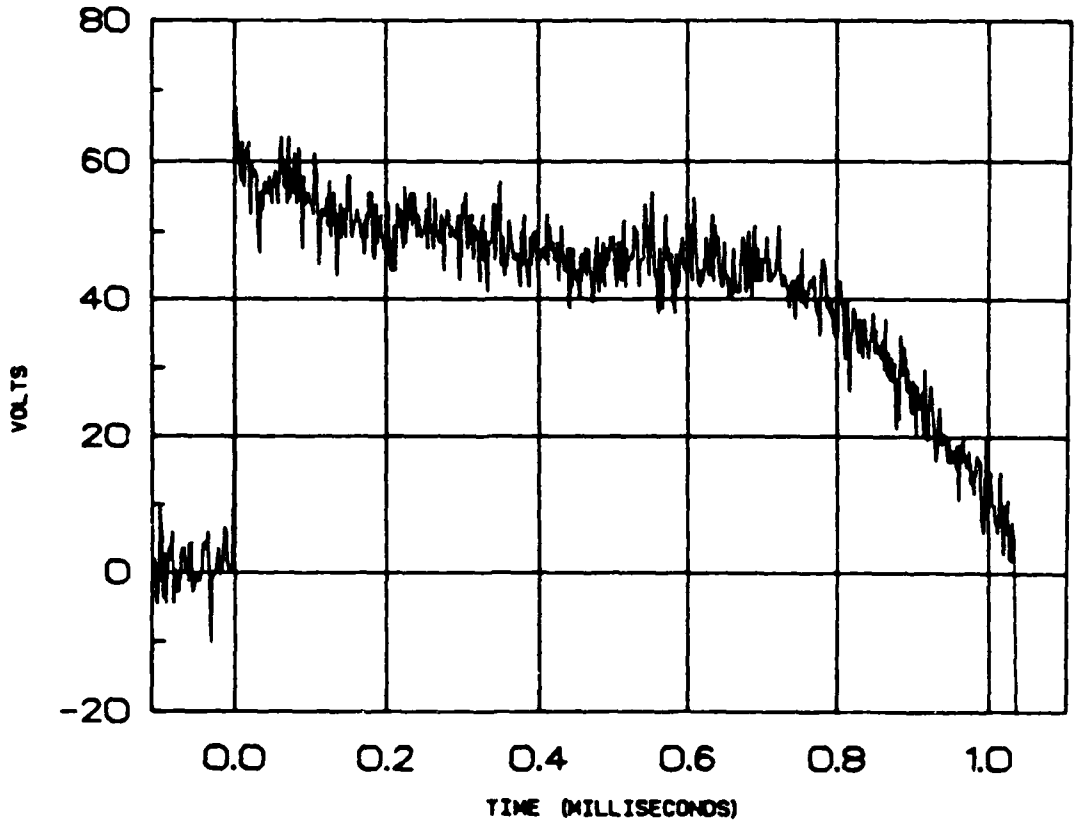

Figure 3. Breech voltage attains a quasi-equilibrium value for approximately 400 μs about 200 μs after current initiation.

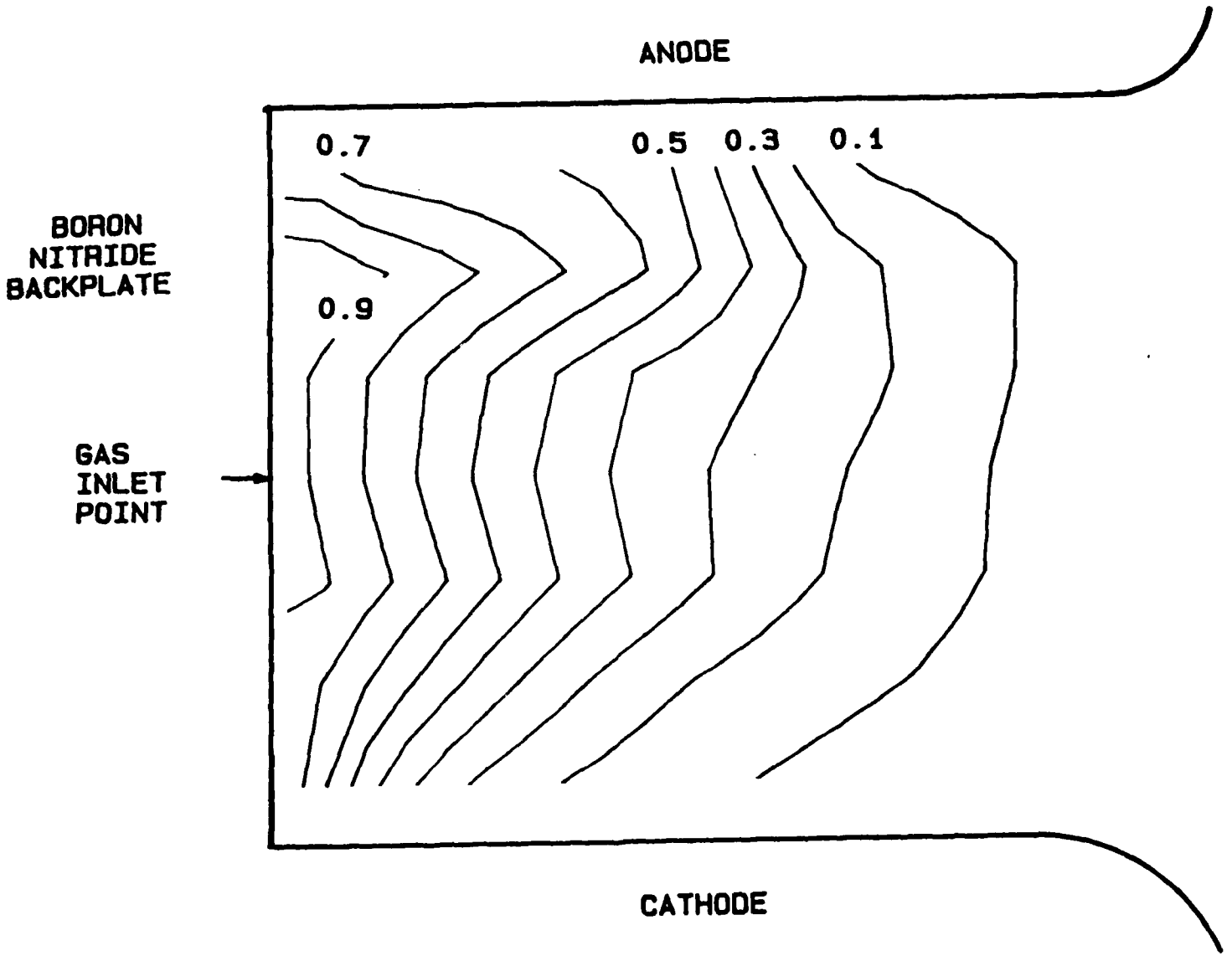

Figure 4. Enclosed current contours from B-probe measurements indicate that the current is largely retained within the thrust chamber and has radial components of $\bar{j} \times \bar{B}$ force toward the conductor walls.

A computer-controlled, time- and spatially-resolved spectrographic system, shown schematically in Figure 5, was used for ion temperature and electron density measurements. In order to make measurements within the arcjet thrust chamber, a slit 1.6 mm wide was machined in the outer conductor at a position 22.7 mm from the boron nitride backplate that allowed observation between the cathode and anode. To minimize the perturbing effects on the current distribution by the slit a series of 4 identical slits were made symmetrically in the outer conductor. These slits are shown schematically in Figure 6. Time integrated line profile measurements were made of the argon ion 434.803 nm line and the 696.28 nm line of hydrogen (H_α).

If the velocity component of a radiating particle parallel to the direction of observation is v_s, then the wavelength appears to be shifted due to the Doppler effect by the amount

$$\delta\lambda_D = \pm \frac{v_s}{c}\lambda_o \tag{1}$$

where λ_o is the unshifted wavelength [2]. If the particle velocities of a radiating system have an equilibrium thermal distribution, then Doppler broadening results in a Gaussian line shape and the observed intensity distribution is Gaussian shape given by

$$I\ (\Delta\lambda) = \frac{I_t}{\sqrt{\pi}\ \Delta\lambda_D} \exp\left[-\left(\frac{\Delta\lambda}{\Delta\lambda_D}\right)^2\right] \tag{2}$$

where $\Delta\lambda_D = \frac{\upsilon}{c}\lambda_o$; $\upsilon = (2kT/\mu)^{\frac{1}{2}}$ is the most probable velocity of the particles, and I_t represents the total line intensity. The full width at the half-maximum intensity point (FWHM) is given by

$$\Delta\lambda_{\frac{1}{2}} = 2\sqrt{\ell n 2}\ \Delta\lambda_D = 1.665\ \Delta\lambda_D$$
$$\Delta\lambda_{\frac{1}{2}}/\lambda_o = 7.713 \times 10^{-5} \sqrt{\frac{T}{\mu}} \tag{3}$$

where T is in eV and μ is the reduced mass [2,3].

The time integrated line profile of 434.803 nm argon ion observed through the slit in the outer conductor was digitally

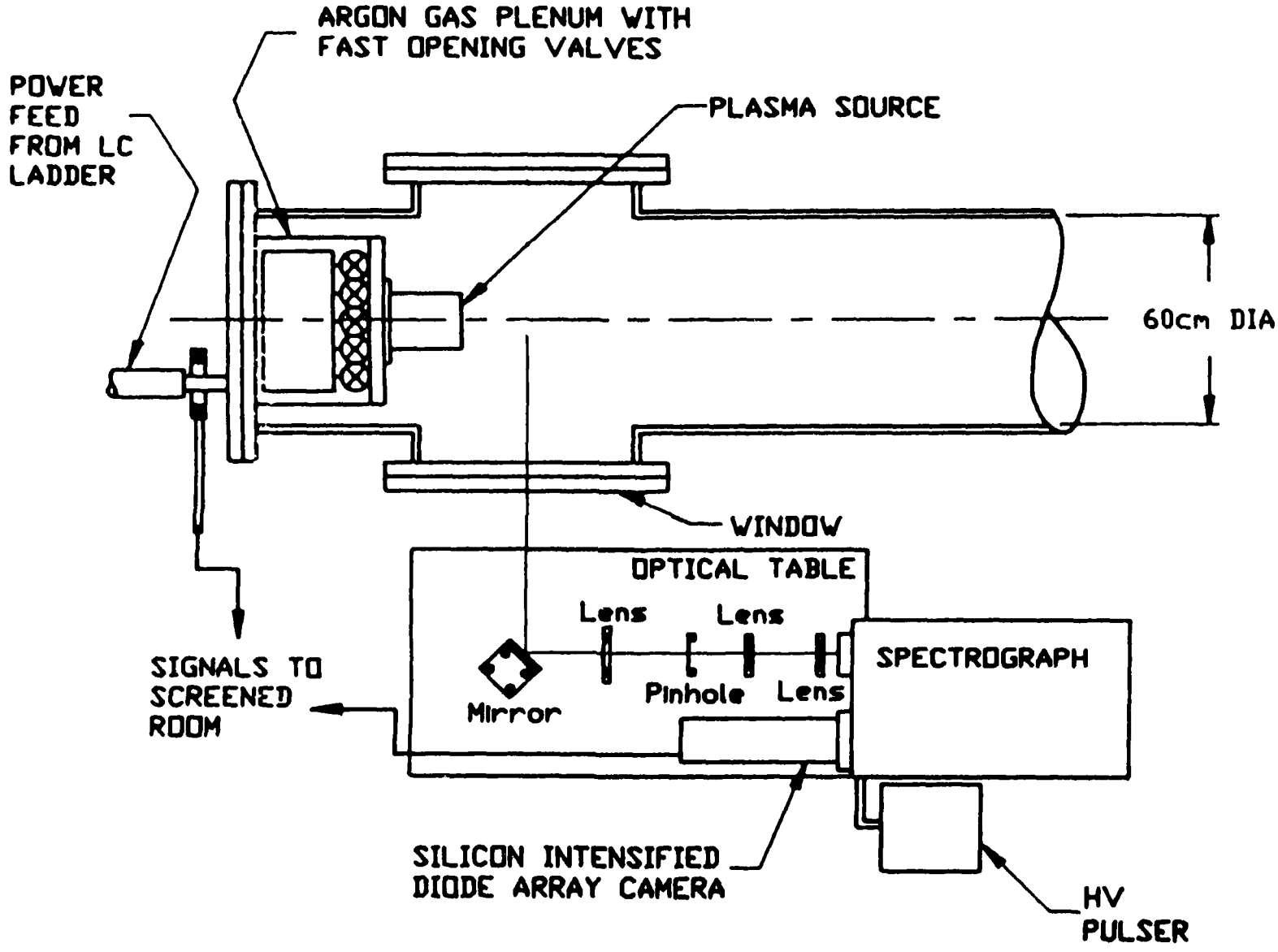

Figure 5. Schematic of MPD arcjet facility showing optical layout for the time- and spatially-resolved digital spectroscopic system.

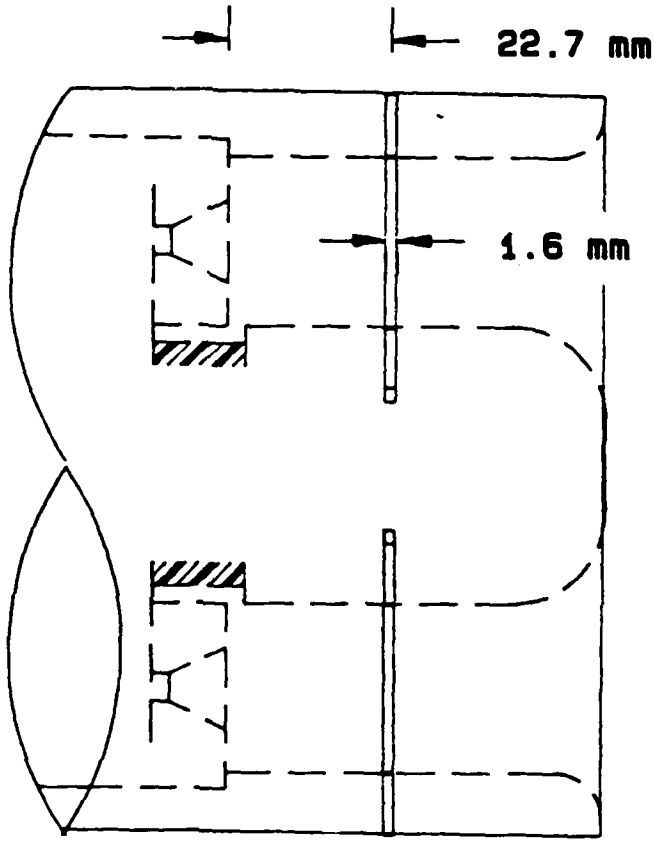

Figure 6. Spectroscopic measurements were made internal to arcjet through a 1.6 mm slit in the outer conductor at the midplane. Four symmetrical slits were cut in the outer conductor to minimize slit effect on current distribution. (This figure depicts arcjet with cathode and midplane injection of mass flow).

recorded with the spectrograph in second order with the entrance slit at 30 microns. The system resolution was 0.002216 nm/pixel with a measured instrument profile that was Gaussian with a FWHM of 0.01262 ± 0.00045 nm. The digital data is intensity integrated over the line of sight versus wavelength and versus spatial position with spatial resolution of 267 microns. The raw data was filtered versus wavelength with a low frequency bandpass filter with frequency cutoff determined by the allowable spectral frequencies from the instrument profile. The data was then filtered spatially with a frequency cutoff of 0.35 cycles/mm. The observed line profile was then Abel-inverted to yield local radial line profiles. These line profiles were then fitted to a Gaussian and the FWHM calculated. Figure 7 shows the relative integrated intensity versus radial position from the Abel inversion. Figure 8 shows the Gaussian fit at 13.6 mm from the cathode with a FWHM of 0.02274 nm with an error of ± 0.00066 nm. Correction for instrument profile yields a FWHM of 0.0189 nm which corresponds to an argon ion temperature of 12.7 eV +0.9 eV. Figure 9 shows the resultant corrected FWHM versus distance from the cathode and Figure 10 indicates the inferred ion temperature versus distance from the cathode. These inferred ion temperatures are very high and are approximately 10 times the electron temperature.

Line profile measurements were also made of hydrogen 696.28 nm line. Hydrogen comprised 1.5 percent of the species injected and at the operating conditions interior to the arcjet the hydrogen is over 90 percent ionized. Thus, the observed hydrogen line intensity was very low and required the sum of 30 shots to yield reasonable statistics. The raw data was filtered and Abel-inverted in the same manner as the argon data. Figure 11 shows the relative integrated intensity versus radial position from the Abel inversion. The original objective was to use the measured argon ion temperature and assume that the hydrogen was in thermal equilibrium, then deconvolve the hydrogen profile using the calculated Doppler contribution. The deconvolved profile would then be fitted to a Lorentzian profile to yield electron density from Stark broadening calculations. The

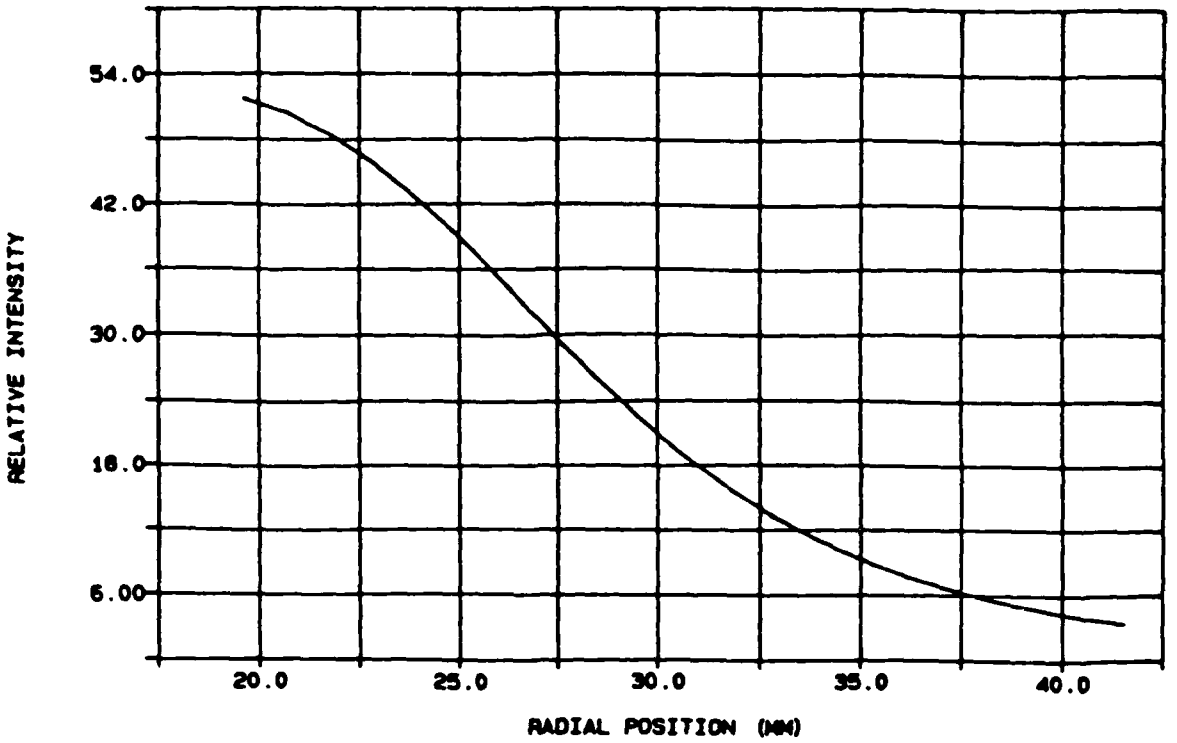

Figure 7. Relative intensity of argon ion emission versus radial position from Abel inversion of ArII 434.803 nm emission is peaked toward the cathode (at 19.05 mm) and monotonically decreases.

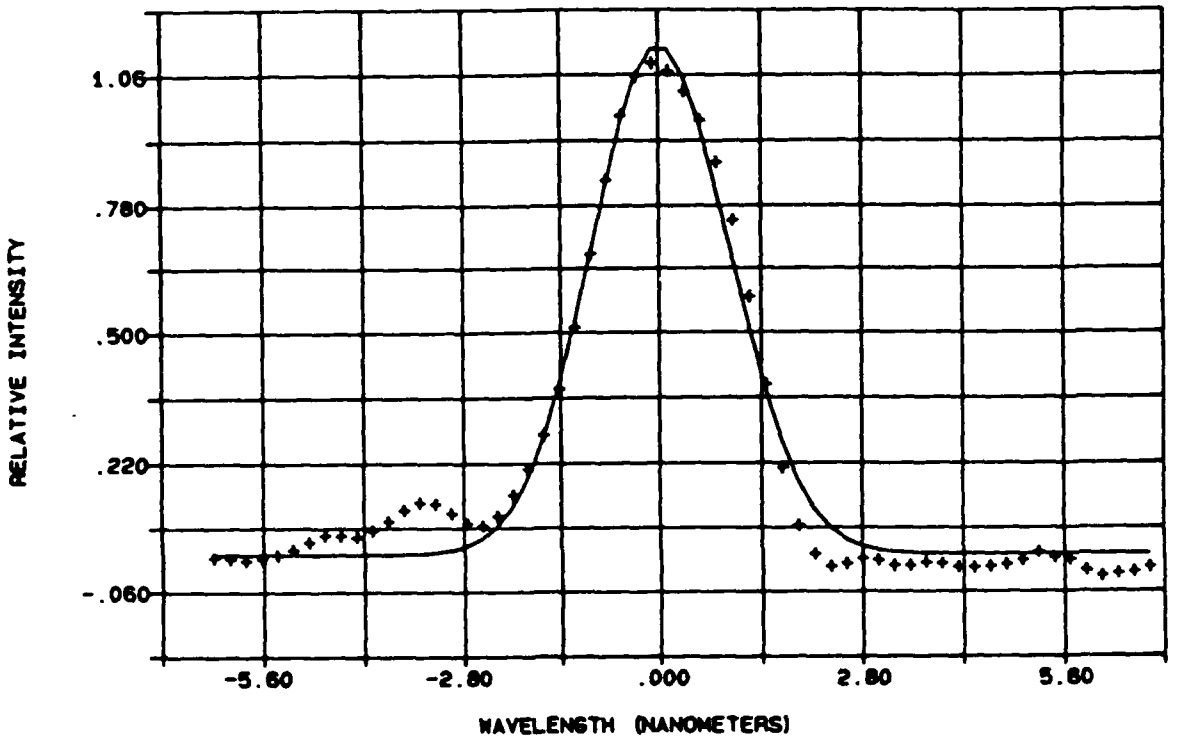

Figure 8. Line profile of Ar II 434.803 nm emission at 13.6 mm from the cathode shows a reasonable fit to a Gaussian profile.

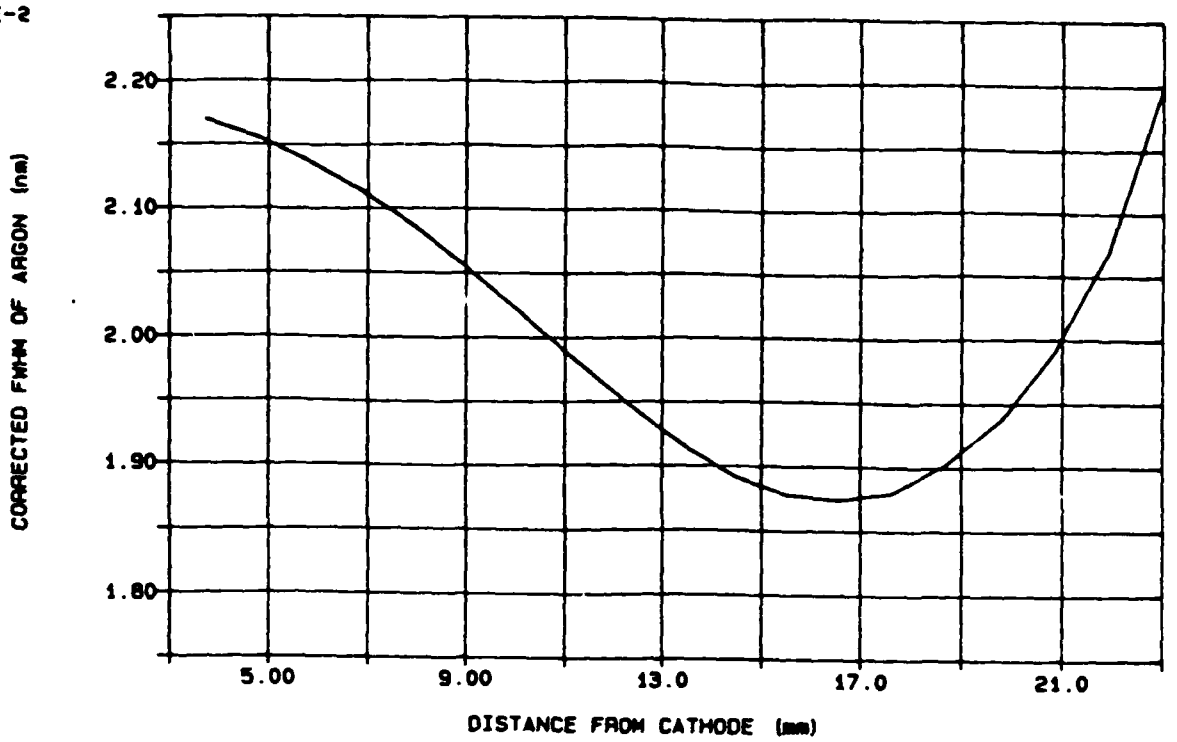

Figure 9. Calculated FWHM versus distance from cathode from argon ion emission profiles fitted to a Gaussian line profile and corrected for instrument profile.

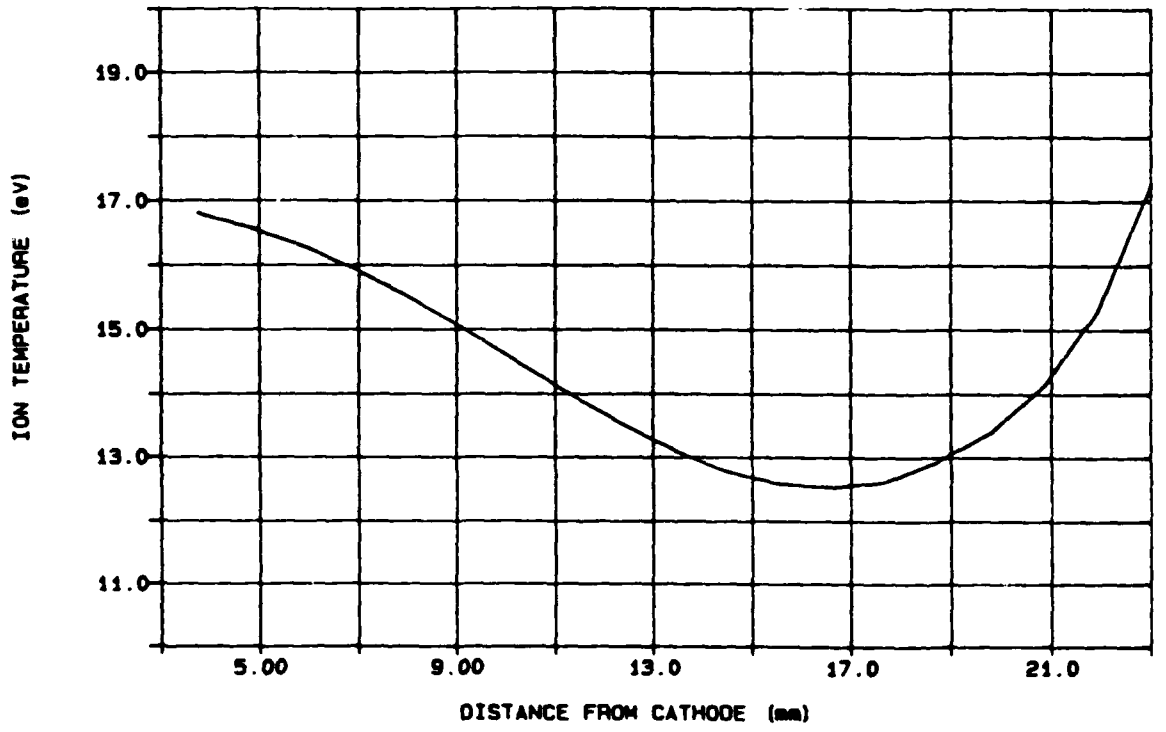

Figure 10. Calculated argon ion "temperature" versus distance from the cathode from corrected FWHM measurements of line profiles.

technique was not possible since most of the line profile was dominated by Gaussian components but with calculated FWHM much less than necessary to equal the argon ion "temperature". The observed Abel-inverted hydrogen profile was therefore fitted to a Gaussian and to a Lorentzian simultaneously. The accuracy of this method is not as good as if the two broadening mechanisms could be separated. However, regions existed where there was no apparent Lorentzian contribution and had a good fit to a Gaussian thus allowing a method to start the dual fit. Figure 12 shows the calculated hydrogen temperature from a fit to the Gaussian contribution. These temperatures are certainly more reasonable than calculated from the argon ion line profiles with a peak calculated temperature of only 0.85 eV. A fit to a Lorentzian component in the hydrogen profile only occurred within 10 mm of the anode. The resultant calculated electron density is shown in Figure 13. Note that significant errors in the calculation of the Lorentzian contribution (i.e., 50 percent) can be tolerated and still yield a reasonable measure (factor of 2) of the electron density.

If the particle density inside the channel is approximately $2 \times 10^{15}/cm^3$ and the electron temperature is on the order of 1.2 - 1.5 eV then the hydrogen and argon are over 90 percent ionized. The coulomb collision frequency of hydrogen ions (protons) and argon ions yields relaxation times for thermal equilibrium of tens of nanoseconds. The ion-neutral relaxation times for the same species are significantly longer, on the order of 100 - 200 ns but are still less than the expected residence time of flow particles in the thrust chamber. One therefore expects better coupling between the hydrogen atoms and the argon ions than indicated in Figures 10 and 12. The calculation of atom temperature assumes a Maxwellian distribution of velocities characteristic of that temperature. Doppler broadening may not be necessarily a consequence of random particle motion, but can also occur as a consequence of collective motion in separate regions of the plasma sampled in the line of sight. In this case, since the spectrograph accepts light from different regions of the plasma that may be moving in complicated ways, the

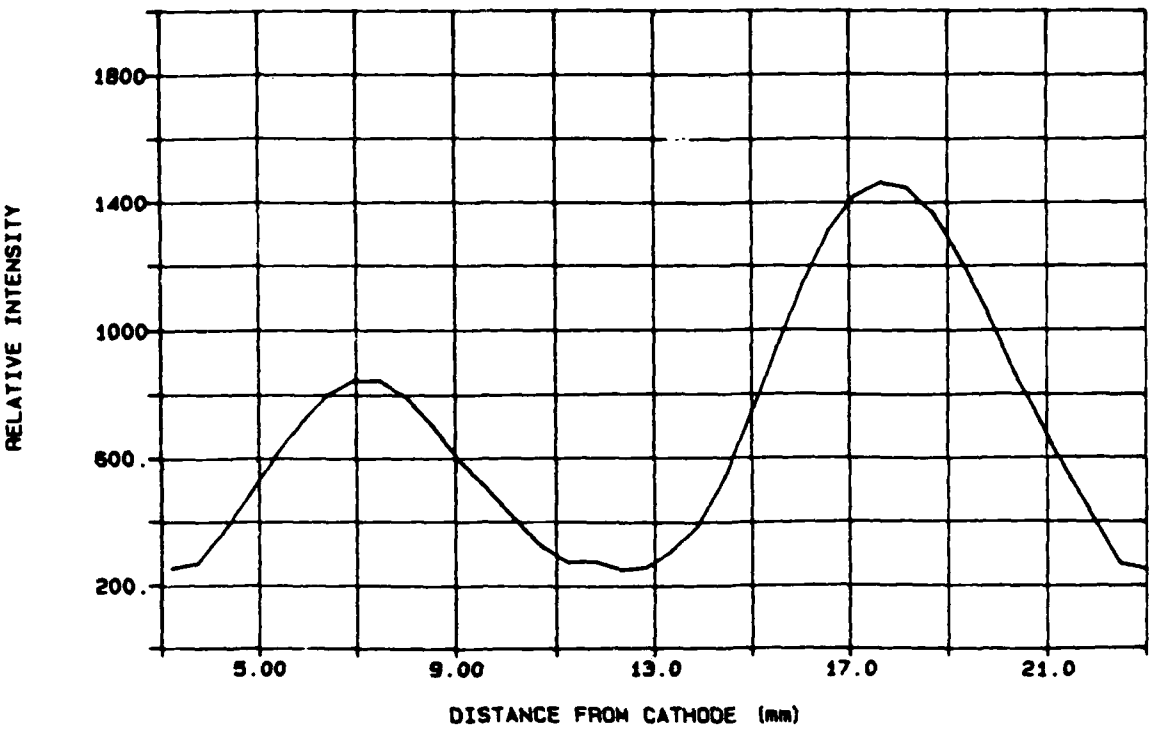

Figure 11. Relative intensity of hydrogen emission versus distance from the cathode from Abel inversion of H_α 696.28 nm emission.

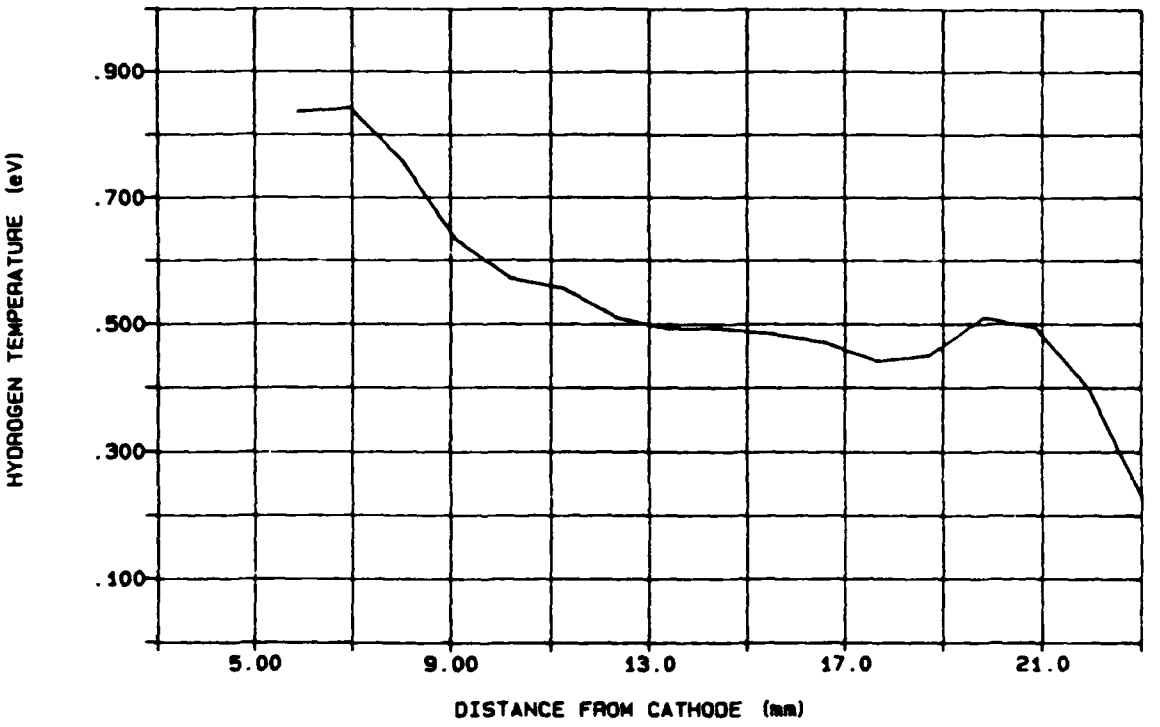

Figure 12. Calculated hydrogen temperature versus distance from the cathode from Gaussian component of line profile fit to hydrogen 696.28 nm emission.

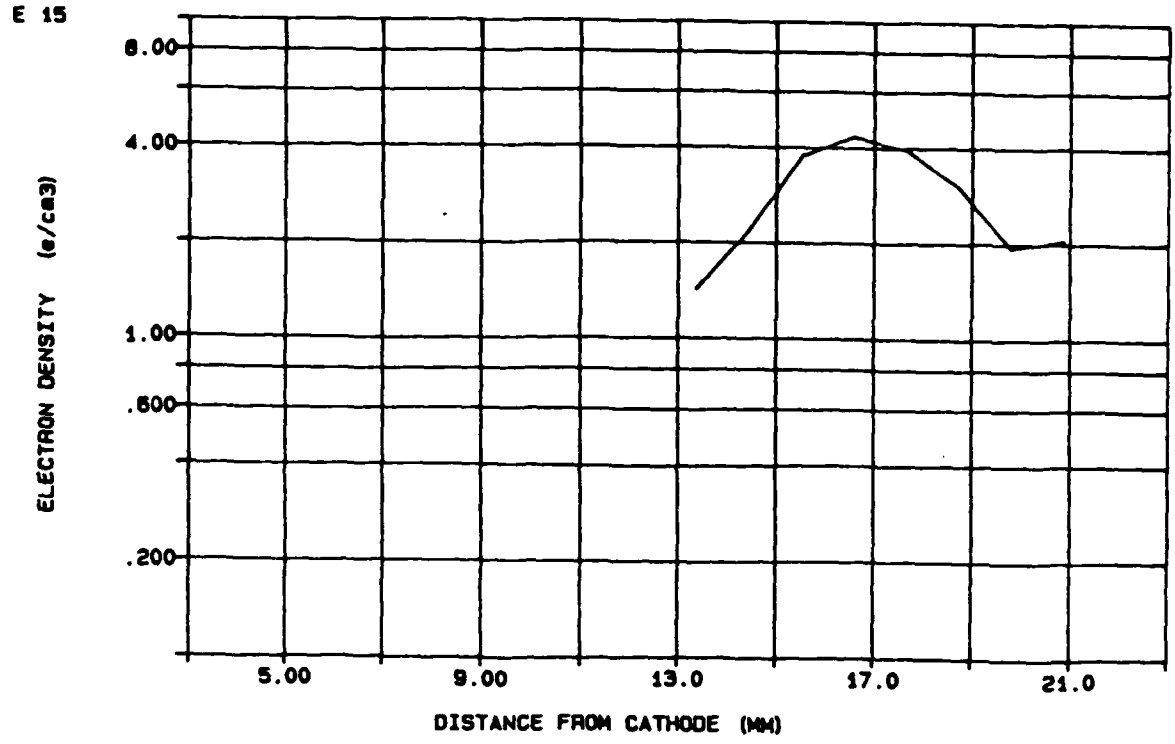

Figure 13. Calculated electron density versus distance from the cathode from Lorentzian component of line profile fit to hydrogen 696.28 nm emission.

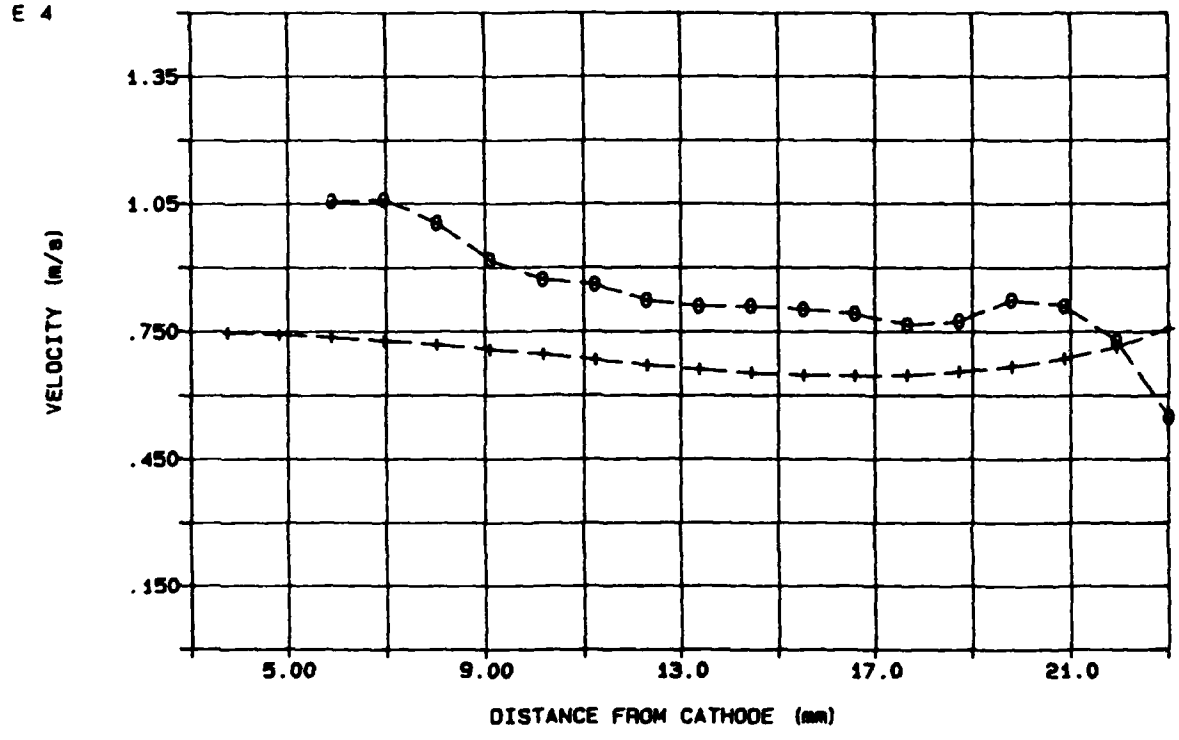

Figure 14. Average relative macroscopic velocity component along the line of sight from FWHM measurements of Gaussian line profiles of argon ion (+) and hydrogen atom (0) emissions with no assumed effects due to kinetic temperature.

analysis of the line shape cannot show whether the broadening is a consequence of the thermal motion of the ions or atoms or whether it is due to a distribution of radial flow (including fluid turbulence). There is the possibility that the observed Doppler broadening of the argon and hydrogen is due to unresolved macroscopic motion which may result in Gaussian profiles. In this case, the average relative macroscopic velocity component along the line of sight is related the line profile width by

$$\langle V_r \rangle_{av} = \frac{c}{2\sqrt{\ell n 2}} \frac{\Delta\lambda_{\frac{1}{2}}}{\lambda_o} \qquad (4)$$

and has nothing to do with the kinetic temperature in the formula for the usual Doppler width [4]. If this is assumed to be the case for the observed hydrogen and argon profiles then the average relative velocities would be equal. Figure 14 is a plot of velocity versus distance from the cathode for hydrogen and argon using equation 4) and assuming no contribution to the line profile due to effects of kinetic temperature. The rough agreement of average relative velocities between hydrogen and argon tends to imply that the mid-channel kinetic temperature is low with the presence of significant macroscopic motion or fluid turbulence.

Examination of the boron nitride backplate after many shots indicated that cathode material was being deposited on the insulator surface. Such depositions could contribute to erratic arc behavior and might also distort the basic current distribution within the thrust chamber. The gas inlet through the boron nitride backplate was therefore redesigned, as shown in Figure 15, to provide more uniform gas injection. Using the same operating conditions as with the previous design (i.e., 8 kV charge on the PFN and 6 g/s) the line profile measurements of the argon ion at 434.803 nm were repeated with observation through the same mid-channel slit. Figures 16a, b, and c are contour plots of equal intensity versus wavelength versus radial position for a) the raw data, b) smoothed data, and c) Abel inverted data. The smoothed data clearly show line broadening near the cathode but the Abel inversion lost the true line profile.

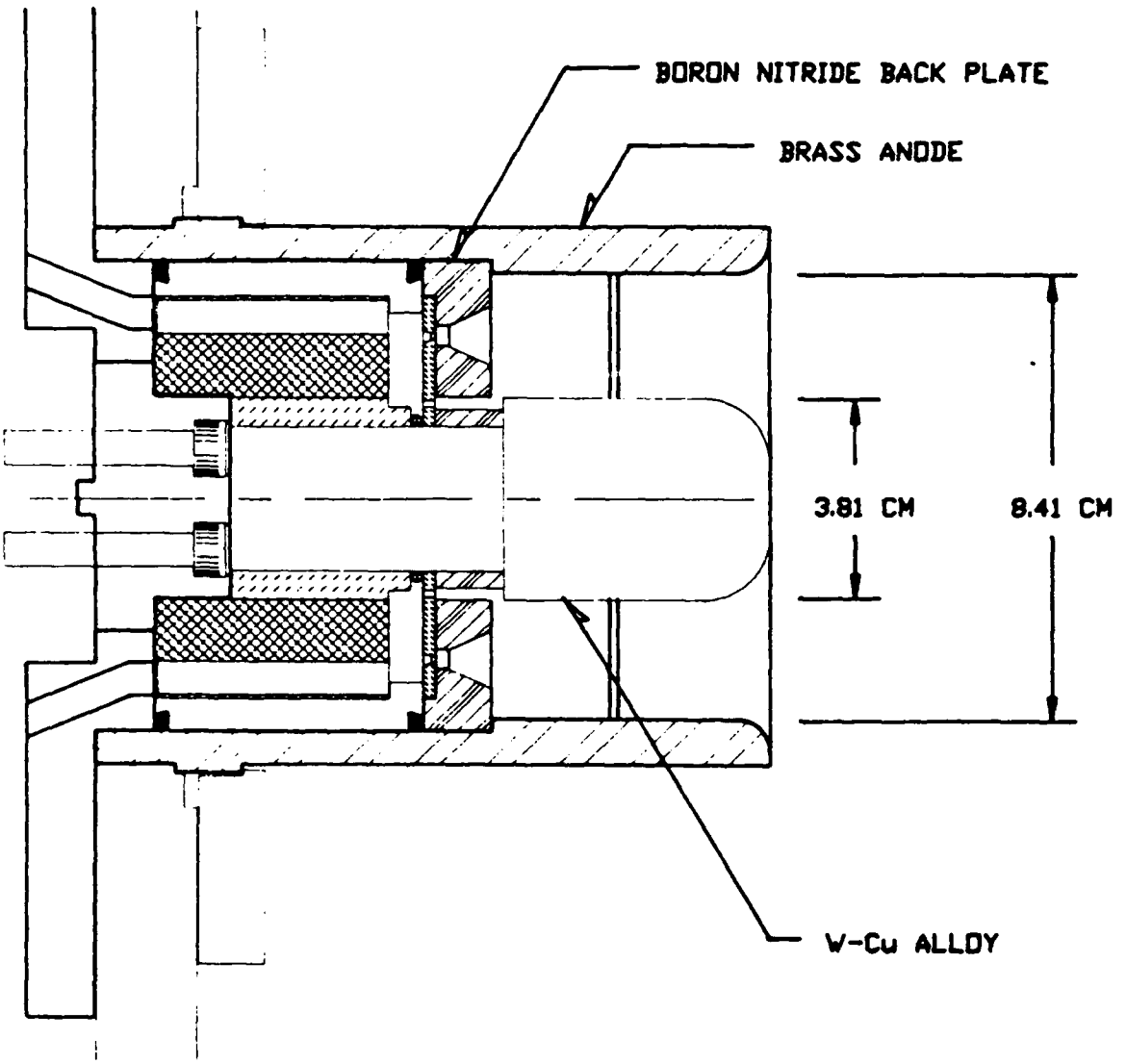

Figure 15. Redesign of gas feed for MPD arcjet with gas injection from 16 nozzles at mid-radius through backplate and equal gas injection from a channel at cathode insulator interface region.

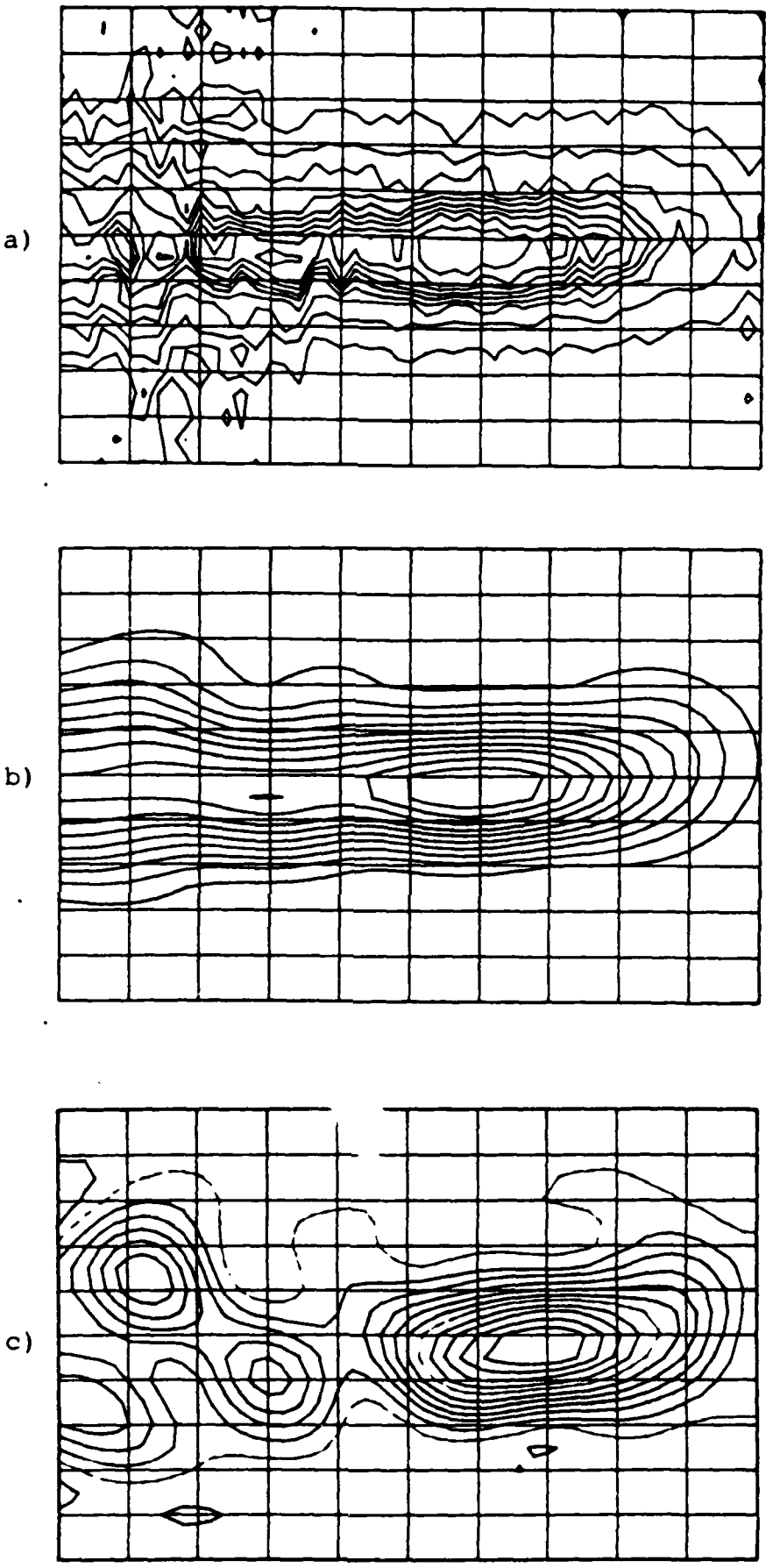

Figure 16. Equal intensity contour maps of ArII 434.803 nm emission observed through slit in outer conductor. The cathode surface is on the left, the anode surface on the right, with 2.17 mm/div horizontal and 0.004434 nm/div vertical. Figure a) raw data, b) smoothed data (note that peak intensity is between 10.8 - 15.2 mm from the cathode), c) Abel inverted data.

Figure 17 shows the wavelength integrated relative intensity versus distance from the cathode. This result differs significantly from the result with the previous design shown in Figure 7. Again fitting the observed line profile to a Gaussian and assuming a Maxwellian velocity distribution yields the ion temperature versus distance from the cathode as shown in Figure 18. The dotted line in Figure 18 at 0.3 eV represents the estimated minimum detectable ion temperature. No detectable ion temperature was observed between 7 - 19 mm from the cathode (note that the electrode gap is 23 mm). In a region within 3 mm of the anode (outer conductor) the ion temperature rises to approximately 2 eV. Near the cathode, the ion temperature rises to above 2 eV by 6 mm, but due to problems with the Abel inversion the accuracy in this region is low.

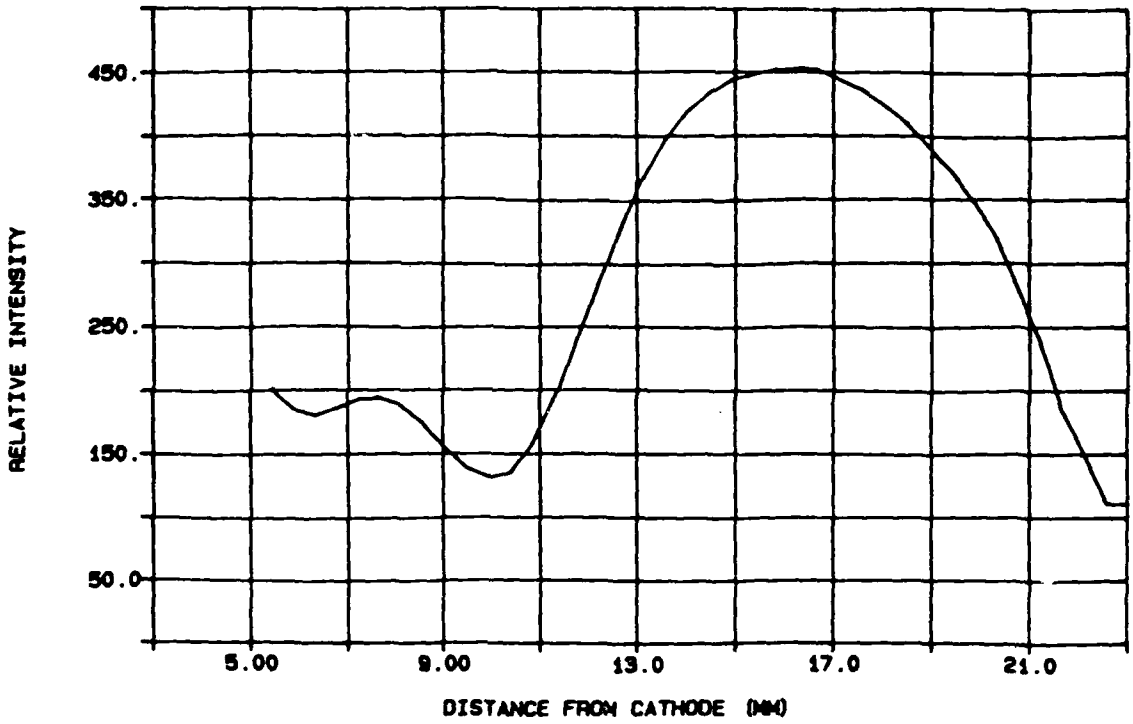

Figure 17. Relative intensity versus distance from the cathode from Abel inverted ArII 434.803 nm emission with new gas inlet geometry.

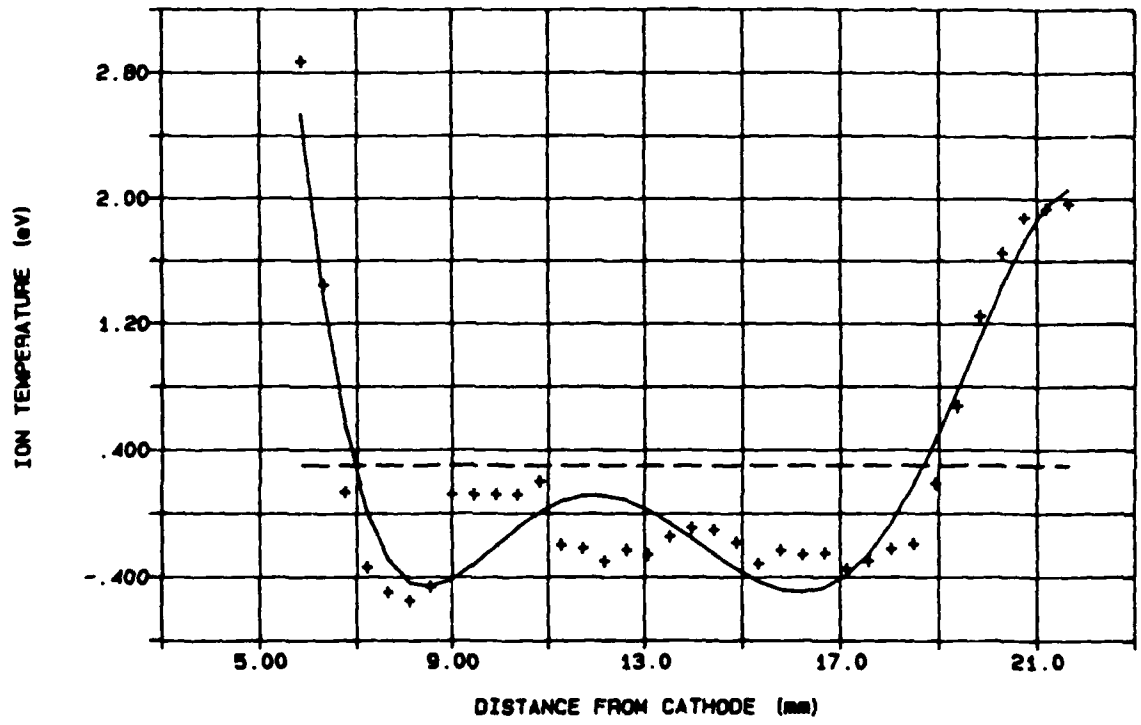

Figure 18. Calculated ion temperature versus distance from cathode from Gaussian fit to Abel inverted line profile of ArII 434.803 nm emission. The dashed line at 0.3 eV represents minimum detectable temperature.

IV. CONCLUDING REMARKS

The experimental program to date has provided strong indications that the flow within the MPD arcjet chamber can be dramatically affected by the choice of inlet geometry. In particular, it appears that introduction of mass flow near the cathode base can offset the development of a strong radially-inward flow. Such flow, as suggested by the linewidth measurements in argon and hydrogen, would have important consequences for thrust efficiency since shock and viscous losses near the cathode surface would be expected. The present measurements are comparisons at the same total current but with an abrupt variation of mass flow distributions by changing the geometry of the mass injection arrangement. It may be expected that the relative strength of the radial (vs axial) flow can change significantly as the total current and mass flow values are varied with fixed injection geometry. Such change in flow direction can substantially affect the MPD thruster performance for reasons that cannot be inferred from simple scaling relationships based on electromagnetic thrust and total mass flow. Examination of MPD performance by variation of operating current and mass flow rate, (i.e. external parameters) with a fixed device geometry will thus be inaccurate for prediction of potential limitations. Each set of external parameter choices may require a particular arrangement of mass injection, electrode geometry and length in order to achieve optimum performance. Internal flow measurements and MACH2 calculations in the next year should provide considerable insight for determining the best combinations of thruster geometry and operating conditions.

V. REFERENCES

1. J. Buff, et. al., "Simulations of a plasma flow switch", in IEEE Transactions on Plasma Science, December 1987, pp. 766-771.

2. W. L. Wiese, in Plasma Diagnostic Techniques, eds. R. H. Huddlestone & S. L. Leonard, Academic Press, New York, 1965. Chapter 6, "Line Broadening", pp. 265-317.

3. G. Traving, in Plasma Diagnostics, ed. W. Lochte-Holtgreven, North-Holland publishing company. Amsterdam, 1968. Chapter 2, "Interpretaion of line broadening and line shift", pp. 66-134.

4. H. R. Griem, Plasma Spectroscopy. McGraw-hill, NY, 1964, Chapter 4, "Line-broadening calculations", pp. 63-103.